buildings

MDPI

Article

Reinforcement Design of a Complex Hydropower Stay-Ring Support Structure: A Comparative Assessment of Simplified Calculations and Three-Dimensional Finite Element Analysis

Yang Zhang [1], Ting Ni [1,*] and Hao Wen [2,*]

[1] College of Environment and Civil Engineering, Chengdu University of Technology, Chengdu 610059, China
[2] PowerChina Guiyang Engineering Corporation Limited, Guiyang 550081, China
* Correspondence: niting17@cdut.edu.cn (T.N.); wen1218hao@163.com (H.W.)

Abstract

The concrete support structure beneath a bottom-dismantled turbine stay ring is a geometrically complex load-bearing region in hydropower powerhouses. Large maintenance openings, variable section thickness, and interaction among the stay ring, spiral case, and surrounding concrete produce three-dimensional load transfer that conventional member-based calculations struggle to represent. This study compares simplified structural calculations and three-dimensional finite element analysis (FEA) for reinforcement design. In the simplified approach, the spatial concrete structure is idealized as planar frames, cantilever corbels, and fixed-end beams, and reinforcement is determined from sectional internal forces according to hydraulic concrete design provisions. A three-dimensional solid model is established in ANSYS, and reinforcement demand is evaluated using an elastic tensile-stress-region approach. For the stay-ring corbel, the simplified calculation gives a required reinforcement of 4926 mm^2/m, whereas the FEA-based tensile-stress-region assessment gives 3079 mm^2/m, corresponding to a reduction of about 37% relative to the simplified result. For the maintenance-gallery roof slab, the simplified calculation gives 4908 mm^2/m, whereas the FEA-based assessment gives 3273 mm^2/m, corresponding to a reduction of about 33% relative to the simplified result. These differences are mainly attributed to spatial restraint and load redistribution in the three-dimensional model. In practical design, the simplified calculation provides a transparent, code-based baseline for load-path definition and sectional reinforcement design, whereas the 3D FEA provides spatially resolved tensile-demand information for checking and refining reinforcement in geometrically disturbed regions; the two methods are therefore complementary.

Keywords: hydropower powerhouse; stay-ring support structure; reinforced concrete; finite element analysis; reinforcement design; simplified calculation; load transfer

Check for updates

Academic Editor: Giuseppina Uva

Received: 19 September 2026
Revised: 16 October 2026
Accepted: 19 October 2026
Published: 4 November 2026

Copyright: © 2026 by the authors. Licensee MDPI, Basel, Switzerland. This article is an open access article distributed under the terms and conditions of the Creative Commons Attribution (CC BY) license.

1. Introduction

Hydropower powerhouse structures contain several reinforced-concrete regions in which concentrated equipment loads, large openings, embedded steel components, and abrupt geometric changes generate complex three-dimensional force-transfer mechanisms. One representative example is the concrete support region beneath the stay ring of a bottom-dismantled hydraulic turbine. In such an arrangement, sufficient space must be reserved below the turbine for inspection, removal, and hoisting of large components. This requirement results in substantial openings and locally reduced structural sections around the stay ring and spiral case, while the same concrete region must simultaneously transfer

loads from the generator pier, turbine, stay ring, spiral case, and associated equipment to the lower powerhouse structure. Consequently, the stay-ring support region differs fundamentally from a conventional beam, slab, or corbel and is more appropriately regarded as a geometrically disturbed three-dimensional load-transfer region. Recent reviews on RC discontinuity regions have summarized the main design tools for such D-regions, including strut-and-tie models, nonlinear FEA and stress-field-based procedures [1,2]. Wei et al. [3] proposed a seismic resistance method for reinforced concrete structures in agricultural water conservancy projects. However, most applications remain two-dimensional or localized, and three-dimensional D-regions with large openings and strong restraint are less covered.

In routine structural design, such complex concrete regions are commonly transformed into mechanically interpretable members, including frames, corbels, deep beams, and slabs. This member-based idealization has important practical advantages because the assumed load path is explicit, sectional actions can be calculated using conventional structural mechanics, and reinforcement can be determined directly in accordance with design-code provisions. Similar simplified structural models have been widely used in engineering practice, and their value lies particularly in transparency, computational efficiency, and ease of independent checking. However, when a continuous concrete region contains large openings, irregular boundaries, embedded structural components, and strong spatial restraint, the reduction from a three-dimensional continuum to one- or two-dimensional members inevitably requires assumptions regarding effective span, support conditions, load distribution, and force-transfer paths. These assumptions can affect the resulting internal forces and, ultimately, the reinforcement demand.

Three broad themes emerge from the literature relevant to the present study. The first theme is the application of refined finite element analysis to complex hydraulic and civil concrete structures. Wan and Xiao [4] employed ANSYS to investigate the structural behavior and stability of a complex surge-chamber system, and Zhang et al. [5] examined the stress response and fatigue life of steel spiral cases in pumped-storage power plants. Recent studies on spiral case structures have further simulated contact nonlinearity, temporary internal water pressure and gap-closing behavior [6,7], while Zhao et al. [8] investigated the stability and strengthening of spiral-case-encased concrete. Zhou et al. [9] analyzed hydro-mechanical interaction and conditional lining–rock cooperation in high-pressure hydraulic tunnels. These studies demonstrate that FE models can represent irregular geometry and complex loading conditions with a high level of detail. However, their primary outputs are stability indices, stress distributions, fatigue life, internal-water-pressure sharing, gap closure or cracking risk, rather than reinforcement demand. Wang et al. [10] combined experimental study and numerical simulation for steel reinforced CA-UHPC one-way slabs, further demonstrating the value of integrating refined numerical models with physical testing. Moreover, they generally do not compare the numerical results with conventional member-based design calculations, and therefore their implications for code-based reinforcement decisions remain indirect.

The second theme concerns the combined use of simplified structural models and finite element analysis. Jia et al. [11] combined simplified structural calculation and FE analysis for frame-supported ribbed-grid composite slab structures, and Tan et al. [12] developed and validated FE models for concrete wind-turbine towers under combined compression and bending. Yoat and Lantsoght [13] compared AASHTO LRFD simplified procedures with linear FEA for skewed slab bridges and found that the two approaches led to different reinforcement layouts and steel weights. These studies demonstrate the value of hybrid or comparative approaches, but the structural systems considered are relatively regular and are dominated by beam, slab, or shell action. They do not address highly disturbed three-dimensional regions with large maintenance openings, embedded steel

components, and multiple interacting load paths. Thoma et al. [14] and Gall et al. [15] further advanced nonlinear FE simulation for reinforced-concrete slabs and segmental tunnel linings, respectively. Their work provides important insight into nonlinear material and construction-stage response, but it focuses on post-test reproduction or lining behavior rather than on the design chain from simplified sectional forces to reinforcement demand in a complex hydropower structure.

The third theme is stress-field-based reinforcement design for discontinuity regions. Stress-field- and strut-and-tie-based reinforcement design for D-regions has been extensively reviewed [1,2]. Liu et al. [16] linked tensile stress regions obtained from structural analysis to reinforcement design in anchorage zones. Nie et al. [17] developed a strut-and-tie model and reinforcement design method for gussets in containment vessels, while He et al. [18] combined full-scale testing and a strut-and-tie model for thick-plate multiple-block anchorage zones. These studies confirm that tensile-stress or strut-and-tie approaches can provide a rational basis for reinforcement in D-regions where conventional sectional forces are difficult to define. However, they are typically limited to localized regions and often rely on two-dimensional or strut-and-tie idealizations. They do not examine full three-dimensional load redistribution in a stay-ring support structure or compare the resulting reinforcement demand with that obtained from conventional member-based design.

Taken together, the existing literature leaves a clear research gap. First, most refined FE studies of hydropower structures concentrate on stress, deformation, stability, or fatigue, rather than on reinforcement design. Second, studies that do address reinforcement tend to focus on isolated D-regions such as anchorage zones or gussets, and they seldom consider the complete structural system with large openings and strong spatial restraint. Third, although simplified-versus-FEA comparisons exist for bridges and regular slab/beam systems [13], no study has systematically compared, for the same geometrically complex hydropower stay-ring support structure, the reinforcement demand obtained from conventional member-based calculations and from a three-dimensional FEA-based tensile-stress-region assessment. Consequently, how structural idealization influences reinforcement decisions, and how simplified calculations and refined FEA should be combined in practical design, remains insufficiently addressed. This gap motivates the present study.

This gap is particularly relevant to the concrete support structure beneath a bottom-dismantled turbine stay ring. In conventional design, the continuous three-dimensional system can be decomposed into a sequence of idealized structural members, such as a generator pier, a planar frame surrounding the spiral case, a cantilever corbel, and a fixed-end beam representing the maintenance-gallery roof slab. In a three-dimensional continuum model, by contrast, these components remain mechanically connected and can redistribute load through the surrounding concrete. The resulting difference in structural representation may therefore influence both the location and magnitude of the calculated tensile demand and, consequently, the reinforcement required in critical regions.

Against this identified gap, the present study investigates the stay-ring support structure of a large hydropower powerhouse while withholding project-identifying information for confidentiality. Two reinforcement-design routes are examined. The first is a conventional structural calculation in which the continuous concrete region is transformed into mechanically interpretable members and reinforcement is determined from sectional internal forces in accordance with the adopted hydraulic concrete design provisions. The second uses a three-dimensional finite element model to obtain the elastic stress and deformation fields, from which reinforcement demand is evaluated using a tensile-stress-region approach. The comparison focuses on the lower stay-ring corbel and the maintenance-gallery roof slab because both regions can be independently designed using the two approaches. The contribution of this study lies in three aspects. First, it addresses a structural configuration—the

concrete support region beneath a bottom-dismantled turbine stay ring—that has rarely been reported in the literature and is characterized by large maintenance openings, variable section thickness, and strong spatial restraint from the surrounding mass concrete. Second, it establishes a complete comparison chain from structural idealization through load transfer representation to quantitative reinforcement demand, rather than merely comparing stress distributions. Third, it provides a mechanistic explanation for the observed differences by tracing them to specific modeling choices: the reduction of a 3D continuum to 1D members, the conversion of spatially distributed actions to equivalent line loads, the representation of surrounding restraint as idealized supports, and the transformation of localized tensile stress fields into global sectional actions.

Accordingly, the objectives of this study are threefold: (1) to examine how member-based and three-dimensional continuum representations differ in describing load transfer within a geometrically complex hydropower concrete structure; (2) to quantify the resulting differences in reinforcement demand for the lower stay-ring corbel and the maintenance-gallery roof slab; and (3) to clarify the respective roles and limitations of simplified structural calculation and refined FEA in practical reinforcement design. Rather than proposing a new finite element formulation, this study provides a design-oriented comparative case study that connects differences in structural idealization directly to differences in reinforcement decisions for a rarely reported hydropower structural configuration.

2. Engineering Case and Design Conditions

2.1. Structural Configuration

The investigated structure is located in the turbine-unit region of a large hydropower powerhouse. To preserve project confidentiality, the project name, geographical location, and other identifying information are not reported. The powerhouse adopts a bottom-dismantled turbine arrangement, in which sufficient space must be reserved beneath the turbine for inspection, removal, and hoisting of major components during maintenance.

The concrete structure beneath the stay ring forms a critical part of the turbine support system. It transfers loads from the generator pier, turbine components, spiral case, stay ring, and associated equipment to the lower powerhouse structure and foundation. At the same time, the maintenance requirements introduce large internal openings and locally reduced structural sections beneath and around the stay-ring region. These geometric characteristics result in a structurally disturbed zone with pronounced three-dimensional load transfer and local stress concentrations.

The principal structural components considered in this study include the generator pier and wind enclosure, the concrete surrounding the steel spiral case, the stay-ring support region, the lower annular corbel, and the roof slab of the maintenance gallery. These components are mechanically interconnected in the actual structure but are represented at different levels of abstraction in the two design approaches examined in this study. In the conventional calculation, they are simplified into mechanically interpretable members, whereas the finite element model retains their three-dimensional geometric continuity.

2.2. Design Basis and Material Properties

The structural analysis was conducted using the general-arrangement drawings of the powerhouse, turbine-manufacturer information, and the design provisions adopted in the original engineering project. The principal design standards adopted in the original engineering project were the Code for Design of Hydraulic Concrete Structures (DL/T 5057-2009) [19] and the Code for Load Design of Hydraulic Structures (DL/T 5077-1997) [20]. It should be noted that DL/T 5057-2009 [19] has since been superseded by NB/T 11011-2022 [21], which came into effect on 4 May 2023. The original

structural design and the corresponding finite element analysis were completed in 2017, at which time DL/T 5057-2009 was the governing standard in force. The comparison presented in this study is therefore based on the design provisions of DL/T 5057-2009, which is consistent with the standard actually applied in the engineering design.

To assess whether the subsequent code revision could affect the comparative conclusions, the principal differences between the two code versions were examined. In NB/T 11011-2022, the partial factor for permanent actions was increased from $\gamma_G = 1.05$ to $\gamma_G = 1.10$, and the partial factor for variable actions was increased from $\gamma_Q = 1.20$ to $\gamma_Q = 1.30$. However, the material strength design values relevant to this study—specifically the tensile strength design value of C25 concrete ($f_t = 1.27$ N/mm^2) and the tensile strength design value of HRB400 reinforcement ($f_y = 360$ N/mm^2)—remain unchanged between the two code versions. Furthermore, the stress-based reinforcement assessment procedure specified in Appendix D of DL/T 5057-2009 is retained in substance in NB/T 11011-2022. Since both the simplified structural calculation and the three-dimensional finite element analysis adopted the same load combinations and material parameters, an increase in partial factors would proportionally raise the reinforcement demand in both calculation routes without altering the relative difference between them. The comparative findings of this study are therefore not expected to be sensitive to the code version adopted.

The concrete used in the investigated structure is C25, and the reinforcement is HRB400 steel. According to the original project classification, the structure was treated as a Class I hydraulic structure. For completeness and reproducibility, the material and design parameters adopted in both the simplified structural calculation and the finite element analysis are summarized in Table 1. The same material properties, partial factors, and load combinations were used in the two calculation routes so that the comparison reflects differences in structural idealization rather than differences in design input.

Table 1. Load combinations considered in the structural analysis.

Spiral Case Type	Limit State	Combination Type	Operating Condition	Load Name					
				Self-Weight	Generator-Pier and Wind-Enclosure Load	Turbine-Floor Live Load	Internal Water Pressure	External Water Pressure	Temperature Action
Concrete surrounding steel spiral case	ULS	Basic	Normal	√	√	√	—	—	√
			Emptying	√	√	√	—	—	—
	SLS	Standard	Normal	√	√	√	—	—	√
			Emptying	√	√	√	—	—	—

Note: "√" indicates that the corresponding load is considered in the combination; "—" indicates that the load is not considered.

For concrete, the elastic modulus is $E_c = 2.80 \times 10^4$ N/mm^2, Poisson's ratio is $\nu = 1/6 \approx 0.167$, the design compressive strength is $f_c = 11.9$ N/mm^2, the design tensile strength is $f_t = 1.27$ N/mm^2, and the characteristic tensile strength is $f_{tk} = 1.78$ N/mm^2. The nominal unit weight of C25 reinforced concrete is taken as 25 kN/m^3, which is within the normal range for normal-weight concrete and includes the effect of reinforcement in an average sense. It should be emphasized that the value 28.875 kN/m^3 used in the finite element model is not the actual material unit weight. It is an equivalent design self-weight obtained by applying the structural importance factor, design situation factor, and permanent-action partial factor to the nominal unit weight: $\gamma_0 \gamma_G \times 25 = 1.1 \times 1.05 \times 25 = 28.875$ kN/m^3. This value represents the factored permanent action under the ULS basic combination and is used only to apply self-weight consistently with the simplified structural calculation. No additional mass is introduced.

For HRB400 reinforcement, the elastic modulus is $E_s = 2.0 \times 10^5$ N/mm^2, the characteristic yield strength is $f_{yk} = 400$ N/mm^2, and the design tensile and compressive strengths are $f_y = f'_y = 360$ N/mm^2. The nominal concrete cover adopted in the crack-width and detailing checks is $c = 50$ mm.

The structure was designed with cracking permitted and crack width controlled. The crack-control class is Class III, and the maximum allowable crack width is $[w_{\mathrm{lim}}] = 0.30$ mm for the maintenance-gallery roof slab in a Class II indoor moist environment. For the corbel, the crack-control coefficient was taken as $\beta = 0.70$.

The design coefficients adopted in the original project are as follows: structural importance factor $\gamma_0 = 1.1$ for a Class I structure; design situation factor $\psi = 1.0$ for persistent situations; structural coefficient for reinforced concrete $\gamma_d = 1.2$; permanent-action partial factor $\gamma_G = 1.05$; variable-action partial factor $\gamma_Q = 1.20$; and all serviceability limit state partial factors equal to 1.0. The ULS combinations are basic combinations, and the SLS combinations are standard combinations. No additional variable-action combination reduction factor was used; the design situation factor was taken as 1.0. A dynamic amplification factor of 1.5 was applied to the runner-dismantling maintenance load.

The stay ring and steel spiral case were not treated in the same way in the finite element model. The stay ring was represented as an equivalent solid region and therefore contributed stiffness. The steel spiral case was not modeled as a separate stiffness-contributing shell; its cavity was retained, and no internal water pressure was applied to the surrounding concrete because the steel liner was designed to resist the full internal water pressure. Details are given in Section 3.2.2.

The analysis considered the structural response under service and ultimate design conditions associated with normal powerhouse operation and turbine-maintenance activities. The same material grades and principal load combinations were used in both calculation routes to ensure that the comparison reflects differences in structural idealization rather than differences in design input.

2.3. Load Cases and Design Assumptions

2.3.1. Load Cases

Two principal operating conditions were considered in the original structural design: normal operation and spiral-case emptying associated with turbine maintenance. The corresponding load combinations include structural self-weight, loads transferred from the generator pier and wind enclosure, live load on the turbine floor, and temperature action where applicable. Internal and external water pressures were treated according to the structural role of the steel spiral case and the surrounding concrete.

For the turbine-maintenance condition involving downward removal of the runner and rotating components, a dynamic amplification factor of 1.5 was applied to the relevant maintenance load. The adopted ultimate limit state (ULS) and serviceability limit state (SLS) combinations are summarized in Table 1.

2.3.2. Assumptions for the Simplified Structural Calculation

To enable conventional hand calculation, the continuous three-dimensional structure was transformed into a series of simplified structural members. The principal assumptions were as follows.

First, the concrete surrounding the steel spiral case was represented by a planar Γ-shaped frame. One side of the frame was assumed to be supported by the stay-ring region, while the opposite side was restrained by the surrounding mass concrete. The thickness of the equivalent frame was taken as the minimum thickness of the secondary concrete

surrounding the spiral case, and the member length was defined along the section centerline. The corresponding simplified structural representation is shown in Figure 1.

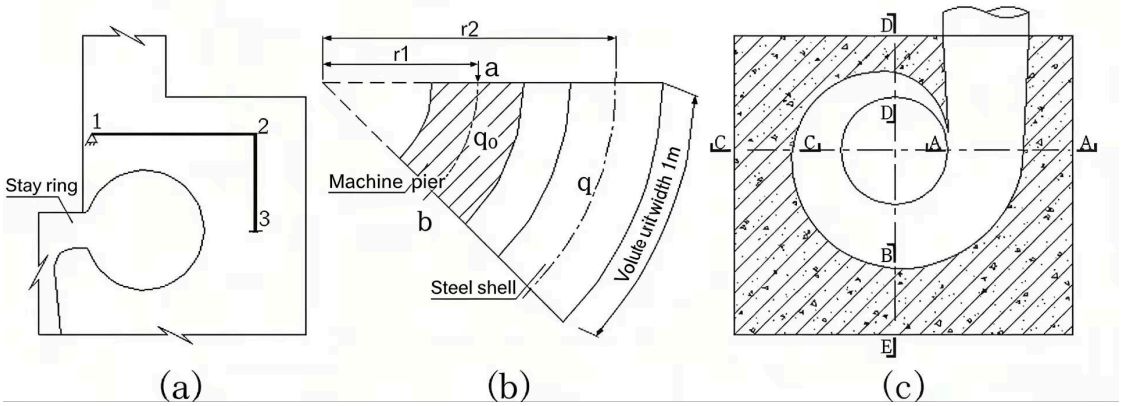


Figure 1. Simplified calculation schematic of the Γ-shaped frame. (**a**) Planar frame model; (**b**) load distribution on the spiral case over a unit width; (**c**) plan view showing the locations of representative sections.

Second, a unit circumferential width of 1 m was adopted for the simplified calculation. Loads transferred from the generator pier were converted into equivalent distributed loads acting on the spiral-case wall or roof region.

Third, because the spiral-case/stay-ring support is circumferentially asymmetric, four representative circumferential sections at 0°, 90°, 180°, and 270° were first selected for preliminary screening. The 0° inlet section has the largest effective span and the most unfavourable load distribution; it was therefore adopted as the governing circumferential section for the subsequent reinforcement calculation. The member-level analyses described in Section 3.1.2 were then focused on the +X and −Y directions, which represent the two extreme wall-thickness and restraint conditions bounding the remaining circumferential sections.

Fourth, the internal hydraulic pressure was assumed to be resisted primarily by the steel spiral case and was therefore not directly included in the surrounding-concrete calculation. The reinforced-concrete structure was designed with cracking permitted, and the serviceability assessment focused on crack-width control.

Finally, for the runner downward-dismantling condition, the weight of the rotating turbine components was included with a dynamic amplification factor of 1.5.

The overall member-based calculation model and the relative positions of the principal structural components are illustrated in Figure 2.

2.3.3. Role of the Simplified Model in the Comparative Assessment

The purpose of the simplified model was not to reproduce the full three-dimensional stress field of the stay-ring support structure. Rather, it provided a transparent engineering representation of the principal load-transfer path and a code-based baseline for reinforcement design. This baseline was subsequently compared with the results obtained from the three-dimensional finite element model.

Accordingly, the simplified and finite element approaches were evaluated using the same engineering case, material properties, and principal loading conditions. The comparison therefore focuses on the influence of structural idealization—particularly the representation of load transfer, support restraint, and local tensile demand—on the resulting reinforcement design.

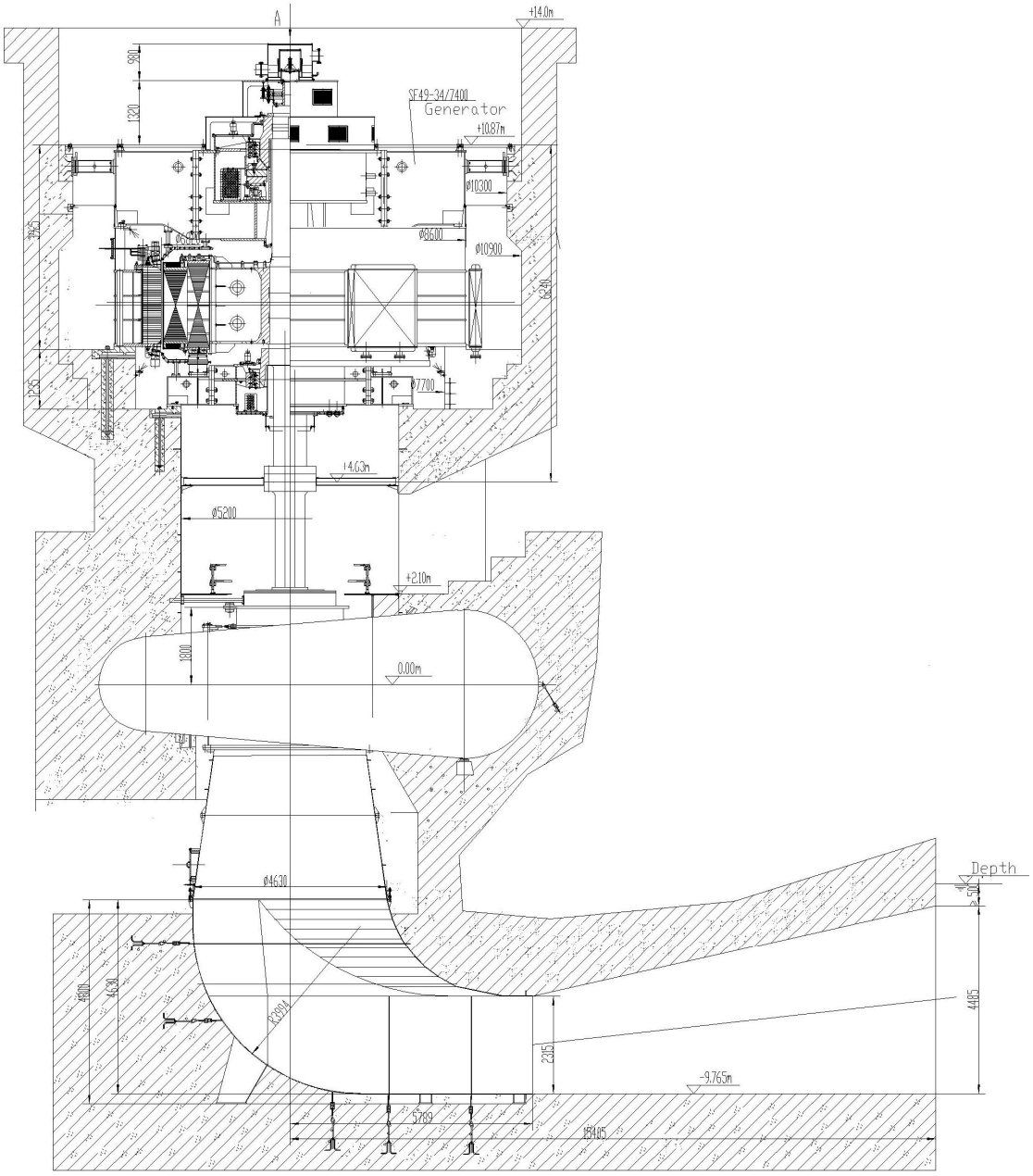


Figure 2. Schematic representation of the member-based calculation model.

3. Research Methodology

3.1. Simplified Structural Calculation

The simplified structural calculation follows the principal load-transfer sequence from the upper powerhouse structure to the lower stay-ring support system. Loads from the wind enclosure, generator pier, turbine components, and associated equipment are first evaluated and transferred to the concrete surrounding the spiral case. The resulting forces are then transmitted to the stay-ring support, the lower corbel, and the maintenance-gallery roof slab. The objective of this calculation route is to obtain sectional internal forces that can be used directly for code-based reinforcement design.

3.1.1. Generator-Pier Load Transfer

The wind enclosure and generator pier are treated as a short cylindrical structural system subjected to vertical and eccentric actions. The considered loads include the self-

weight of the wind enclosure and generator pier, floor loads, fixed generator components, the lower bracket assembly, runner-hoisting loads, rotating components of the generator and turbine, and axial hydraulic thrust. The standard and design values adopted in the calculation are summarized in Table 2.

Table 2. Loads acting on the wind enclosure and generator pier.

Load Type	Standard Value (kN/m)	Design Value (kN/m)
Wind enclosure self-weight	88.63	102.36
Generator pier self-weight	54.4, 38, 156.1	62.83, 43.89, 180.3
Floor load	168.08	216.34
Fixed generator parts	71.75	82.87
Lower bracket assembly	7.28	8.4
Runner hoisting (maintenance)	23.19	26.81
Rotating parts (generator + turbine)	235.72	259.29
Axial hydraulic thrust	280.28	308.31

Based on the resultant vertical force and bending moment at the bottom of the pier, the maximum compressive stress is approximately 990 kN/m^2. For the subsequent spiral-case calculation, this action is converted into an equivalent uniformly distributed load of approximately 484 kN/m^2 acting on the spiral-case roof region.

3.1.2. Spiral-Case Frame and Stay-Ring Reaction

The concrete surrounding the steel spiral case is analyzed using the Γ-shaped frame introduced in Section 2.3.2. Self-weight and turbine-floor live load are applied to the relevant frame segments. The adopted load values are listed in Table 3.

Table 3. Loads applied to the simplified spiral-case frame.

Segment	Load Type	Standard Value (kN/m)	Design Value (kN/m)
AB	Self-weight	30	34.65
BC	Self-weight	75	86.63
AB	Live load	20	26.4

Because the spiral-case/stay-ring support is circumferentially asymmetric, the circumferential direction was screened before the member-level frame analyses were carried out. Four representative sections at 0°, 90°, 180°, and 270° were first compared, as described in Section 2.3.2. The 0° inlet section has the largest effective span and the most unfavourable load distribution, and it was therefore selected as the governing circumferential section for reinforcement design. At the member level, two extreme wall-thickness and restraint conditions were analysed: the +X direction, which represents the thick-wall (3.0 m) and large-span condition, and the −Y direction, which represents the thin second-stage concrete wall (0.8 m, considered together with the downstream first-stage concrete as an equivalent 2.2 m wall) and lower restraint condition. These two directions bracket the main possible load-transfer mechanisms in the simplified frame idealization; they are not intended to imply that the structure is axisymmetric. The +X analysis gives a maximum vertical stay-ring reaction of about 968 kN/m, whereas the −Y analysis gives about 906 kN/m; the +X

direction therefore governs the lower corbel design. The remaining circumferential directions have shorter effective spans and/or more favourable wall/restraint conditions than the governing 0°/+X case and were therefore not carried forward as separate member-level design cases. This selection is consistent with the three-dimensional finite element results, in which the 0° section exhibits the most pronounced tensile demand and the largest vertical deformation. The resulting internal-force combinations for the principal frame segment are summarized in Tables 4 and 5.

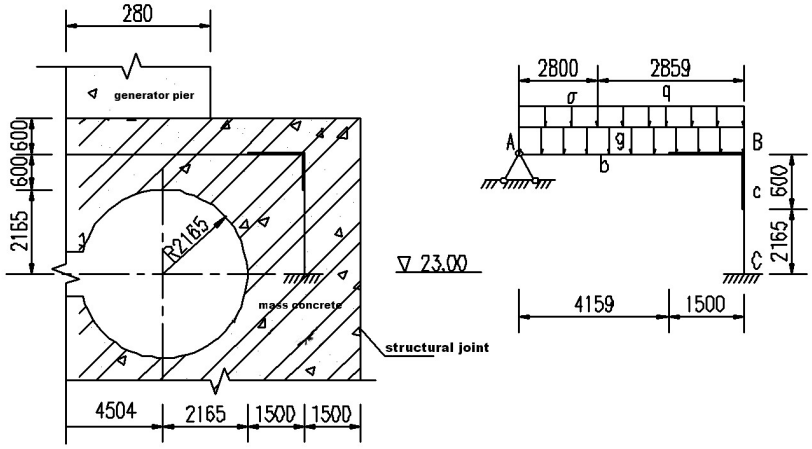
Table 4. Internal-force combinations for segment AB in the +X direction.

Segment	Max + M (kN.M)	Max − M (kN.M)	Max V (kN)
AB	901	−850	968

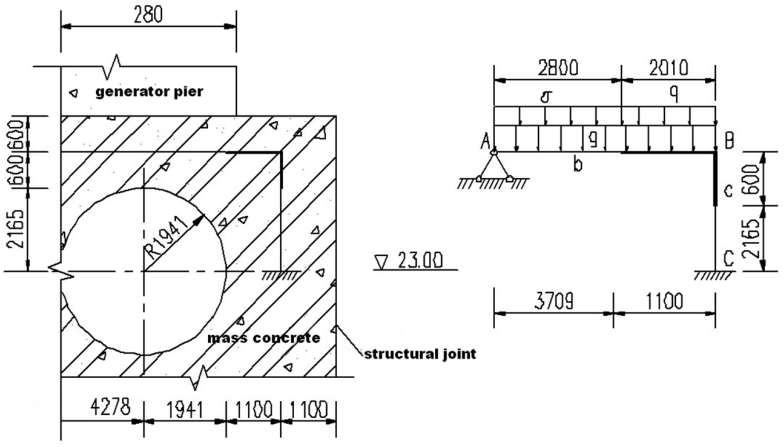
Table 5. Internal force combinations for segment AB (−Y direction).

Segment	Max + M (kN.M)	Max − M (kN.M)	Max V (kN)
AB	790	−664	906

The +X direction governs the design, producing a maximum vertical reaction of approximately 968 kN/m at the stay-ring support, as shown in Figure 3. After the stay-ring self-weight of 30 kN/m and the runner-maintenance load of 24 kN/m are included, the resulting design line load acting on the lower corbel is approximately 1022 kN/m.



(**a**) X direction



(**b**) −Y direction

Figure 3. Simplified spiral-case frame models.

3.1.3. Simplified Modeling of the Stay-Ring Corbel

The design line load obtained from the stay-ring reaction is applied to the lower corbel. In the simplified calculation, the corbel is treated as a cantilever member, and the root section is checked for flexural resistance, shear resistance, local bearing, and crack control. Reinforcement is subsequently determined from the governing sectional forces in accordance with the adopted hydraulic concrete design provisions.

3.1.4. Simplified Model of the Maintenance-Gallery Roof Slab

The maintenance-gallery roof slab is represented as a fixed-end beam supported by the adjacent thick concrete walls. The effective span adopted in the simplified calculation is 5.1 m. The applied actions include the load transferred from the upper corbel together with the self-weight of the roof member. The calculated internal forces are summarized in Table 6.

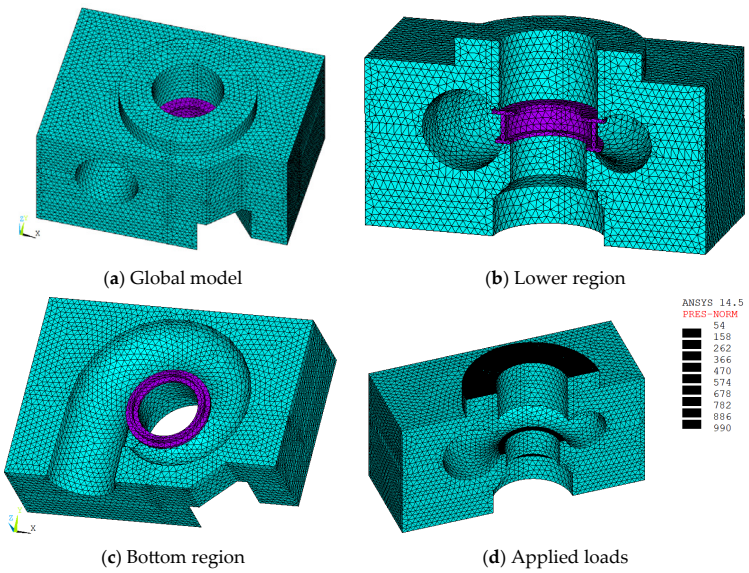
Table 6. Internal forces of the suspended beam.

Corbel Line Load (kN/m)	Span (m)	Beam Self-Weight (kN/m)	Midspan Moment (kN·m)	End Moment (kN·m)	End Shear (kN)
1022	5.1	30	1140	−2280	2683

3.2. Three-Dimensional Finite Element Analysis

3.2.1. Model Configuration

A three-dimensional finite element model was established in ANSYS 14.5 to represent the geometric continuity of the stay-ring support region. Concrete was modeled using SOLID65 solid elements. The stay ring was represented by equivalent solid elements, while the spiral-case cavity and major geometric openings were represented explicitly internal cavities with traction-free surfaces. Floor slabs that were not directly included in the model were accounted for through equivalent applied loads. The overall configuration of the numerical model, together with its lower and bottom portions, is illustrated in Figure 4a–c.



(**a**) Global model (**b**) Lower region

(**c**) Bottom region (**d**) Applied loads

Figure 4. Three-dimensional finite element model and loading scheme.

The global coordinate system was defined with the Y-axis along the flow direction, the X-axis perpendicular to the flow direction, and the Z-axis vertically upward. The overall model dimensions were approximately 12.7 m in the X direction, 18.0 m in the Y direction,

and 7.1 m in the Z direction. These dimensions and the original finite element discretization were retained from the engineering analysis.

The bottom boundary and the downstream side of the model were fully restrained, whereas the remaining external surfaces were left unconstrained in accordance with the original engineering calculation. The applied actions included structural self-weight, equivalent loads transferred from the generator-pier system, and the load acting in the stay-ring region. The loading scheme used in the finite element model is shown in Figure 4d. For clarity, it should be noted that in Figure 4d, the color scale represents the magnitude of the applied distributed loads.

The finite element mesh was generated from the original engineering model and consisted of approximately 211,843 SOLID65 elements and 40,908 nodes. Local mesh refinement was applied to the stay-ring support, the concrete surrounding the spiral case, the lower corbel, and the maintenance-gallery roof slab, while the far-field mass concrete was discretized with a coarser mesh. The material properties used in the FE model were identical to those summarized in Section 2.2: C25 concrete with $E_c = 2.80 \times 10^4$ N/mm^2, $\nu = 0.167$, $f_c = 11.9$ N/mm^2, and $f_t = 1.27$ N/mm^2; HRB400 reinforcement with $E_s = 2.0 \times 10^5$ N/mm^2 and $f_y = 360$ N/mm^2. The stay ring was represented by equivalent solid elements, and the spiral-case cavity and major geometric openings were modeled as voids. Reinforcement was not discretely modeled.

Although a formal mesh-convergence study was not performed, the reinforcement assessment was based on the integrated tensile resultant rather than on the peak nodal tensile stress. This integration reduces the sensitivity of the result to local mesh refinement. The critical sections were selected away from sharp corners and stress singularities. Nevertheless, mesh discretization may affect the predicted extent of the tensile zone and hence the integrated tensile force. The reported reinforcement demands should therefore be regarded as design-level estimates, and a mesh-sensitivity study is recommended in future work.

3.2.2. Material Representation and Analysis Assumption

Concrete was modeled using the SOLID65 element available in ANSYS 14.5. The finite element analysis was conducted within a linear-elastic framework, consistent with the original engineering analysis. This assumption was adopted because the objective of the numerical model was to obtain the design-level stress and deformation fields under the prescribed loading conditions rather than to simulate progressive cracking, stiffness degradation, or ultimate failure.

Within this framework, the calculated elastic stress field was used to identify the principal compression and tension regions within the stay-ring support structure. The tensile stress distribution was subsequently employed in the reinforcement assessment described in Section 3.3. Accordingly, the finite element model is interpreted in this study as a refined continuum representation of load transfer and local stress distribution under the design actions, rather than as a nonlinear prediction of the complete failure process. With respect to the steel spiral case and stay ring, the following modeling assumptions were adopted. The stay ring was represented as an equivalent solid region and therefore contributed stiffness to the finite element model. The separated fixed guide vanes were smeared into an equivalent continuous solid based on the equivalent-stiffness principle, consistent with the original engineering analysis. The steel spiral case was not modeled as a separate stiffness-contributing shell. Because an elastic cushion was provided between the upper half of the steel spiral case and the surrounding concrete, and because the steel liner was designed to resist the full internal water pressure, no internal water pressure was applied to the surrounding concrete. The spiral-case cavity was retained as an internal cavity with traction-free surfaces in the solid model. Reinforcement was not modeled as discrete

elements; the required reinforcement was assessed from the elastic tensile stress field using the procedure described in Section 3.3. It should be noted that the linear-elastic model does not explicitly capture cracking-induced stiffness degradation, tension stiffening, bond-slip, or force redistribution. The computed tensile stresses are therefore elastic indicators for reinforcement assessment rather than actual post-cracking stresses. The computed tensile stresses are therefore elastic indicators for reinforcement assessment rather than actual post-cracking stresses; the implications of this limitation are discussed in Section 5.4.

3.2.3. Boundary Conditions and Applied Loads

The boundary conditions were defined in accordance with the original engineering model. The bottom boundary and the downstream side of the finite element domain were fully restrained, while the remaining three lateral sides and the top surface were left unconstrained. These conditions were intended to represent the restraint provided by the surrounding structural system within the scope of the original engineering analysis.

The applied actions included the self-weight of the concrete structure and the equivalent loads transferred from the upper powerhouse components. The self-weight was applied as a factored design action. As explained in Section 2.2, the nominal unit weight of C25 reinforced concrete is 25 kN/m^3, and the equivalent design unit weight is $\gamma_0 \psi \gamma_G \times 25 = 1.1 \times 1.0 \times 1.05 \times 25 = 28.875$ kN/m^3. This value is not the actual material density, and no additional mass is introduced; it is used only to keep the self-weight consistent with the ULS combination adopted in the simplified calculation. A uniformly distributed load of 990 kN/m^2 was applied to the generator-pier loading region, representing the resultant action transferred from the upper generator-pier and wind-enclosure system. In addition, a distributed load of approximately 54 kN/m^2 was applied to the concrete surface beneath the stay ring. The locations and distributions of these applied actions are illustrated in Figure 4d.

The loads applied in the simplified and three-dimensional FE models were equivalent at the resultant level. In the simplified calculation, localized actions transferred from the generator pier and wind enclosure were converted, according to Saint-Venant's principle, into equivalent concentrated or distributed line loads acting on the idealized frame and corbel; the resultant force and resultant bending moment were preserved. In the FE model, the same actions were applied directly as distributed pressures on the actual loading surfaces: 990 kN/m^2 on the generator-pier loading region, 54 kN/m^2 on the concrete surface beneath the stay ring, and the factored self-weight. Thus, the global force and moment resultants were consistent between the two models, while the local stress distribution in the FE model was closer to the actual load application. This difference is intentional: the simplified model represents the load path through equivalent member actions, whereas the FE model preserves the spatial distribution of the applied loads.

3.2.4. Stress and Deformation Outputs

The finite element analysis was used to obtain the three-dimensional stress and displacement fields of the stay-ring support structure under the prescribed design actions. Both global contour distributions and representative sectional results were extracted to characterize the structural response.

The stress outputs focused on the distribution of compressive and tensile stresses in the concrete, with particular attention to regions surrounding the spiral case, stay-ring support, lower corbel, maintenance-gallery roof slab, and major geometric openings. These results were used to identify localized tensile regions and to determine the representative sections required for the subsequent reinforcement assessment.

The deformation outputs included vertical and horizontal displacements of the overall structure and of the key local regions. These results were used to examine the deformation pattern of the stay-ring support system and to provide a basis for comparison with the simplified structural calculation.

The extracted stress and deformation fields were subsequently used in two ways: first, to characterize the three-dimensional load-transfer behavior of the structure; and second, to support the tensile-stress-based reinforcement assessment described in Section 3.3.

3.3. Reinforcement Assessment Based on Tensile-Stress Regions

The procedure uses the elastic stress field and does not update internal forces for cracking or stiffness degradation. For geometrically disturbed reinforced-concrete regions in which conventional member-based internal forces cannot be readily defined, the reinforcement demand was evaluated from the elastic tensile-stress field obtained from the three-dimensional finite element analysis. This procedure follows the stress-based reinforcement approach specified in Appendix D of DL/T 5057-2009 [19] and is consistent with the tensile-stress-region concept adopted in previous reinforcement-design studies for complex concrete regions [16].

The basic procedure consists of three steps. First, representative sections are selected according to the location and extent of the tensile zones identified from the finite element stress field. Second, the tensile stresses along the selected section are integrated over the effective tensile region to obtain the corresponding tensile resultant per unit width. Third, the required reinforcement area is determined from the tensile resultant using the adopted reinforcement design strength, after which the calculated reinforcement is adjusted where necessary to satisfy practical detailing requirements.

According to the stress-based procedure specified in Appendix D of DL/T 5057-2009, which is retained in NB/T 11011-2022, the required reinforcement for a non-member region was determined from the total tensile force obtained by integrating the elastic tensile stress diagram in the reinforcement direction over the effective tensile region:

$$T = \int_{h_t} \sigma_t(x)\,\mathrm{d}x (\text{per unit width})$$

or, in discretized form,

$$T = \sum_i \sigma_{t,i} \Delta h_i$$

The effective tensile region was defined as the portion of the section where the principal tensile stress acts in the reinforcement direction and remains tensile; compressive stresses were excluded. For the stay-ring corbel, the effective tensile depth was 0.75 of the section depth; for the maintenance-gallery roof slab, it was 0.80, both exceeding two-thirds of the section depth. The required reinforcement area was calculated as

$$A_s = \frac{\gamma_d T}{f_y},$$

where $\gamma_d = 1.2$ is the structural coefficient for reinforced concrete and $f_y = 360$ N/mm^2 is the design tensile strength of HRB400 reinforcement. For the governing 0° section of the stay-ring corbel region, $T = 887.898$ kN/m, giving $A_s = 1.2 \times 887.898 \times 10^3/360 = 2959.7$ mm^2/m. For the maintenance-gallery roof slab, $T = 880.291$ kN/m, giving $A_s = 1.2 \times 880.291 \times 10^3/360 = 2934.3$ mm^2/m. After minimum reinforcement, spacing, crack-control, and detailing requirements were considered, the adopted reinforcement areas were 3079 and 3273 mm^2/m, respectively, as reported in Section 4.3.

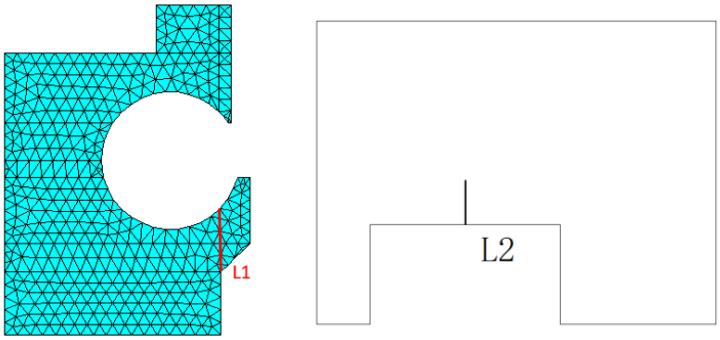
The procedure was applied to two key regions: the lower stay-ring corbel and the maintenance-gallery roof slab. These two regions were selected because both exhibit identifiable tensile zones in the three-dimensional analysis and can also be independently designed

using the simplified member-based approach. This enables a direct comparison between the two reinforcement-design routes at the level of reinforcement demand.

3.3.1. Tensile-Stress Assessment for the Stay-Ring Corbel

For the lower stay-ring corbel, a representative section was selected from the finite element stress field according to the location of the governing tensile region. The tensile-stress distribution along this section was extracted and integrated over the effective tensile depth to obtain the tensile resultant acting per unit circumferential width.

The reinforcement requirement was then determined from the integrated tensile force in accordance with the adopted design provisions. The stress-integration path used for the corbel assessment is illustrated in Figure 5a.



(**a**) Corbel tensile-stress path (**b**) Roof-slab tensile-stress path

Figure 5. Tensile-stress paths used for reinforcement assessment.

3.3.2. Tensile-Stress-Based Reinforcement Assessment for the Maintenance-Gallery Roof Slab

The same stress-based procedure was applied to the maintenance-gallery roof slab. A representative section through the tensile region at the slab bottom was selected from the finite element results. The tensile stresses along the section were integrated over the effective tensile depth to obtain the corresponding tensile resultant per unit width.

The reinforcement demand was subsequently determined from this tensile resultant and adjusted, where necessary, to satisfy practical detailing requirements. The stress-integration path adopted for the roof-slab assessment is shown in Figure 5b.

3.4. Comparative Assessment Framework

The simplified structural calculation and the three-dimensional finite element approach were compared at three complementary levels: structural representation, force-transfer interpretation, and reinforcement demand.

First, the two approaches were compared in terms of structural idealization. The simplified calculation represents the continuous concrete system using mechanically interpretable members, including the Γ-shaped frame, cantilever corbel, and fixed-end beam, whereas the finite element model retains the three-dimensional continuity of the surrounding concrete. Particular attention was given to differences in dimensionality, load idealization, support representation, and the treatment of geometric discontinuities.

Second, the force-transfer characteristics identified by the two approaches were compared. The simplified calculation describes structural behavior through sectional actions such as bending moment, shear force, and support reaction, while the finite element model provides spatial stress and deformation fields. The comparison therefore focused on whether both approaches identify the same critical regions and on how their different structural representations influence the interpretation of local tensile demand and load redistribution.

Third, the reinforcement demand obtained from the two design routes was quantitatively compared for the lower stay-ring corbel and the maintenance-gallery roof slab. For each region, the reinforcement area derived from the conventional member-based calculation was compared with that obtained from the tensile-stress-based finite element assessment. The purpose of this comparison was to evaluate the influence of structural idealization on reinforcement decisions rather than to treat the finite element result as an experimentally validated reference solution.

Based on these three levels of comparison, the subsequent analysis examines both the quantitative differences in reinforcement demand and the mechanical reasons underlying those differences. This framework also provides the basis for discussing the respective roles and limitations of simplified structural calculations and refined finite element analysis in the design of complex hydropower concrete structures.

4. Results

4.1. Results of the Simplified Structural Calculation

The simplified structural calculation establishes a sequential load-transfer path from the upper powerhouse components to the stay-ring support system. The resultant action at the bottom of the generator pier corresponds to a compressive stress of approximately 990 kN/m^2, which is converted into an equivalent distributed load of approximately 484 kN/m^2 acting on the spiral-case roof region.

For the Γ-shaped frame surrounding the spiral case, the +X direction governs the design. The maximum vertical reaction transferred to the stay-ring support is approximately 968 kN/m per unit circumferential length. After including the stay-ring self-weight of 30 kN/m and the runner-maintenance load of 24 kN/m, the resulting design line load acting on the lower corbel is approximately 1022 kN/m. These results are consistent with the load-transfer sequence defined in Section 3.1.

For the lower stay-ring corbel, the governing root section satisfies the adopted ultimate and serviceability design requirements for flexure, shear, local bearing, and crack control. The conventional member-based design results in top longitudinal tensile reinforcement of 8Φ28@250 in two layers, corresponding to a reinforcement area of approximately 4926 mm^2/m. In the strengthened region adjacent to the expansion joint, the spacing is reduced to 150 mm. Additional bent-up bars, stirrups, and distribution reinforcement are provided according to the original detailing requirements.

For the maintenance-gallery roof slab, the fixed-end beam idealization produces a midspan bending moment of approximately 1140 kN·m, a support moment of approximately −2280 kN·m, and an end shear of approximately 2683 kN. The resulting midspan bottom reinforcement is 10Φ25, corresponding to a reinforcement area of 4908 mm^2/m. At the supports, 12Φ32 reinforcement is provided. The calculated maximum crack width remains below 0.29 mm, while the midspan deflection of approximately 1.08 mm is below the adopted limit of 12.75 mm.

The governing calculation sections and the resulting reinforcement details from the simplified design are summarized in Figure 6. In Figure 6, the circled numbers ① to ⑥ are used as bar marks to identify different reinforcement configurations, specifications, and locations. For example, in Figure 6c,d, labels ① and ② denote the top and bottom main longitudinal reinforcement of the slab, respectively, while ③ to ⑥ denote the distribution, stirrup, and side detailing bars. The specific bar diameter, spacing, and arrangement corresponding to each mark are provided in the detailed annotations of the drawings. These bar marks provide a direct reference to the specific reinforcing bars described in the simplified design.

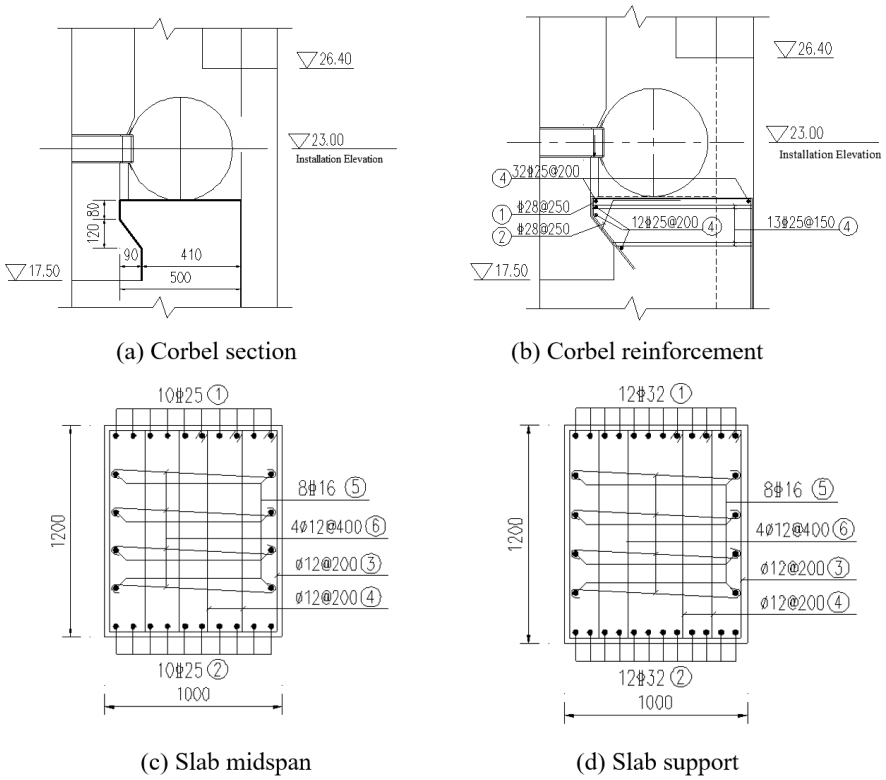


Figure 6. Governing sections and reinforcement details from the simplified structural calculation.

4.2. Three-Dimensional Stress and Deformation Characteristics

4.2.1. Stress Distribution

The three-dimensional finite element results indicate that the stay-ring support structure is predominantly subjected to compression under the prescribed design actions, while localized tensile zones occur around geometric discontinuities, openings, and the stay-ring connection region.

The calculated compressive stress is generally distributed over relatively broad regions of the surrounding concrete. Higher compressive stresses occur around the outer portions of the spiral-case region, with a local maximum of approximately 23.9 MPa near the intersection between the spiral case and the penstock. The compressive stress in the lower stay-ring corbel is comparatively low, while the maintenance-gallery roof slab exhibits increasing compression toward the adjacent side walls. The global and representative sectional distributions are shown in Figure 7. In these contour plots, red indicates regions of high compressive stress, while blue indicates low or zero compressive stress. The stress unit in the legend is kPa.

More importantly for reinforcement design, localized tensile regions are identified around the spiral case, stay-ring support, maintenance gallery, and machine-well openings. The most pronounced tensile region occurs in the concrete between the 0° spiral-case section and the upper stay-ring region, where the calculated tensile stress reaches approximately 7.54 MPa. In the lower stay-ring corbel, the governing tensile region is concentrated near the upper surface adjacent to the spiral-case cavity, with a maximum value of approximately 2.42 MPa. The maintenance-gallery roof slab develops a comparable tensile stress of approximately 2.42 MPa at the bottom of the midspan region. The spatial distribution of these tensile regions is illustrated in Figure 8. In Figure 8, the color gradient from blue to red illustrates the magnitude of the principal tensile stress, where red represents the maximum tensile stress and blue indicates the minimum or compressive stress. The unit for the stress legend is kPa.

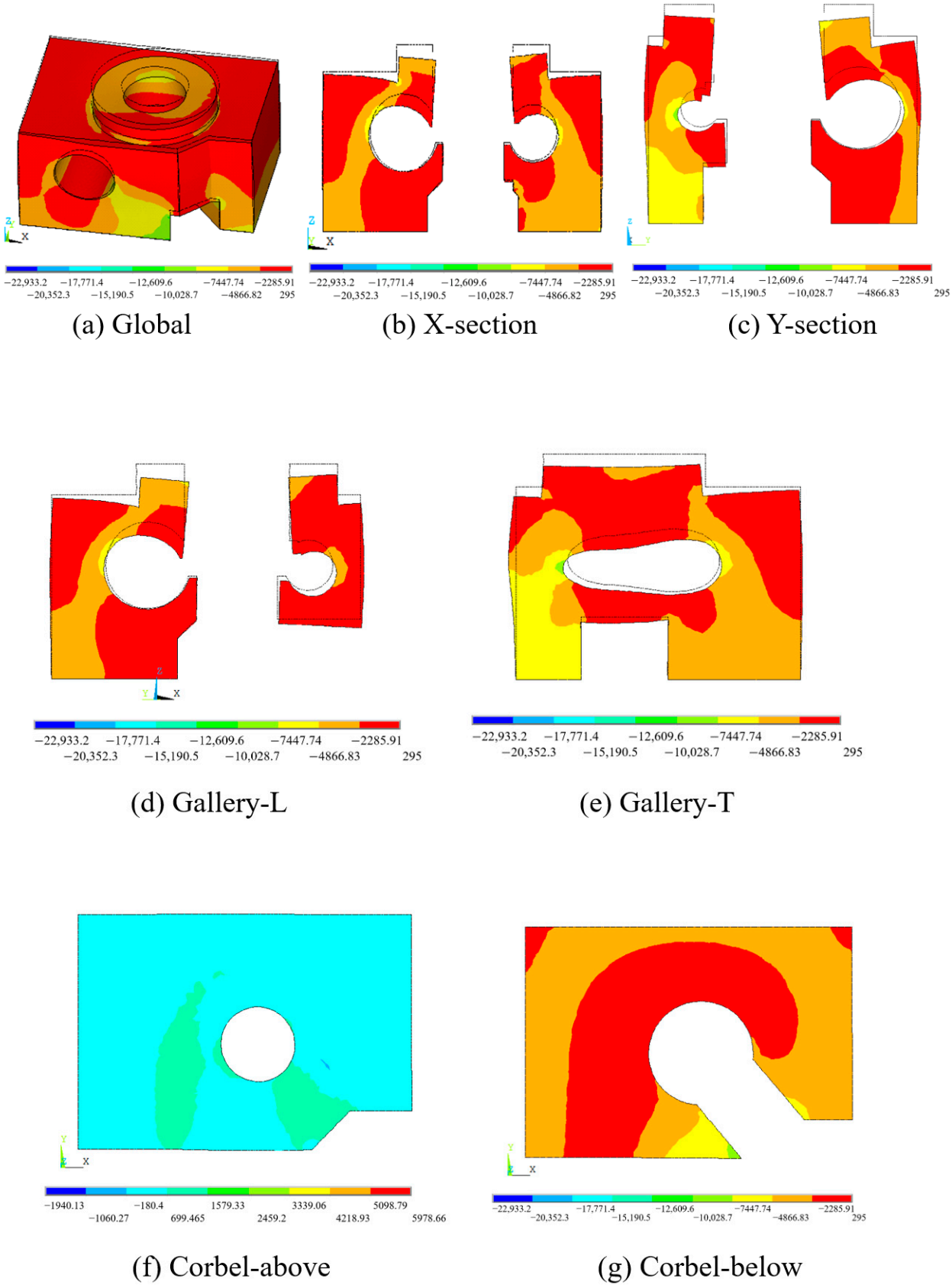


Figure 7. Representative compressive-stress distributions obtained from the three-dimensional model.

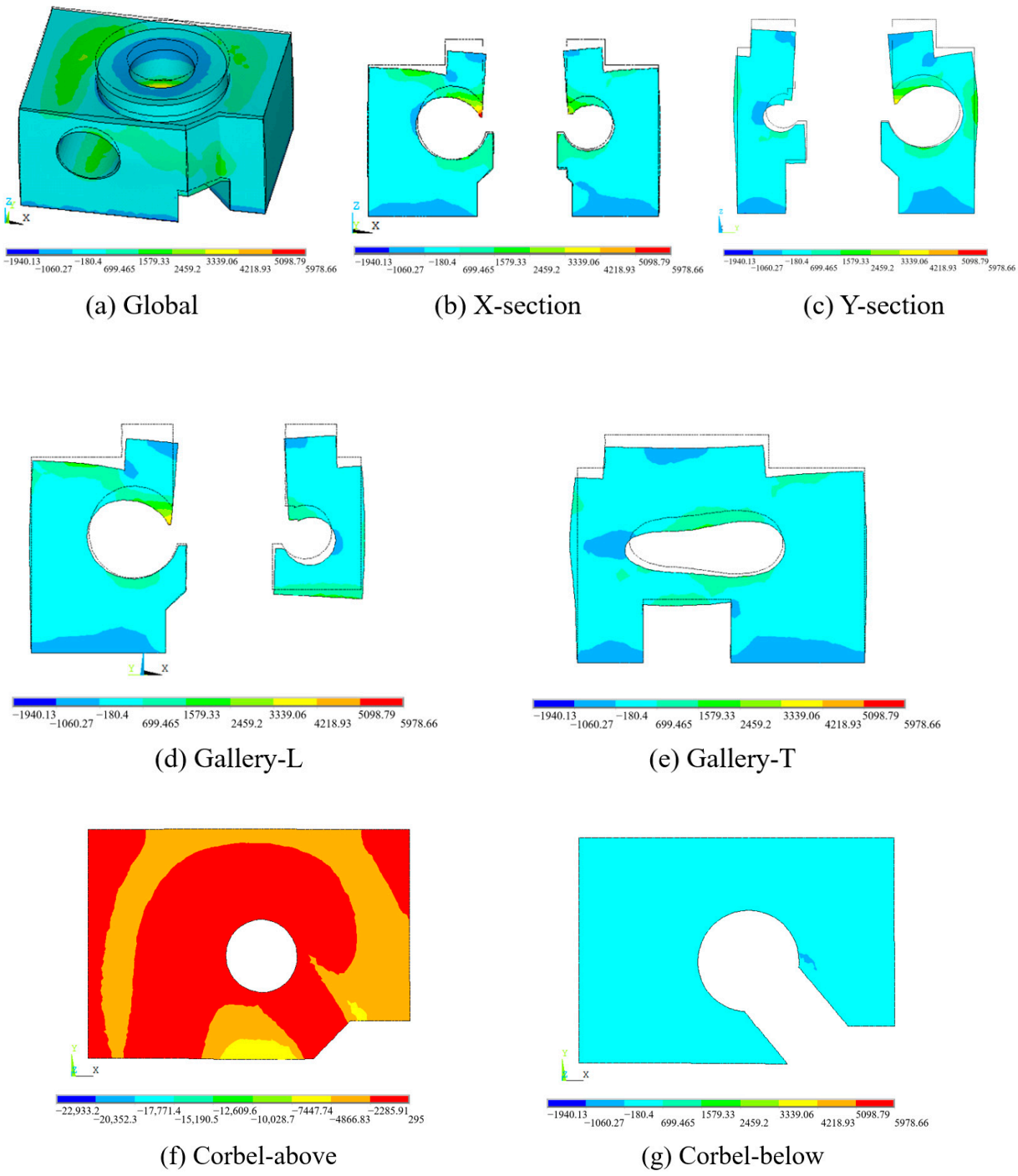


Figure 8. Representative tensile-stress distributions obtained from the three-dimensional model.

The stress results therefore indicate that the dominant tensile demands are strongly localized rather than uniformly distributed over the corresponding member depth. This feature is particularly relevant to the subsequent comparison with the member-based reinforcement design, in which the same structural regions are represented through equivalent sectional forces.

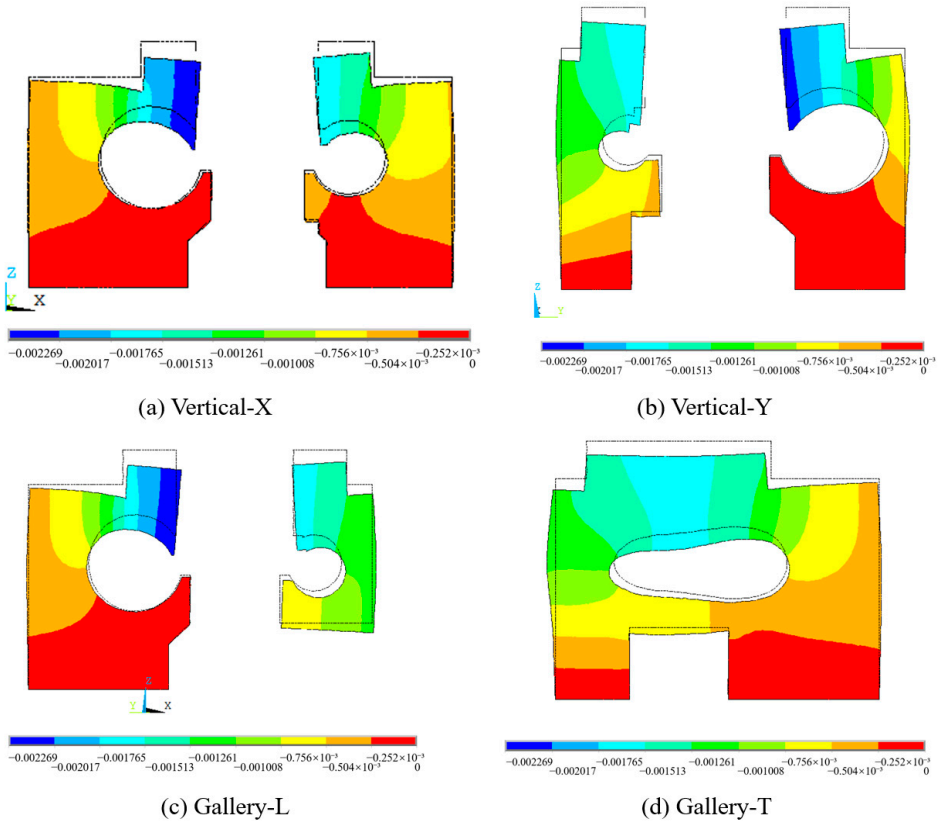
4.2.2. Deformation Characteristics

The deformation field is consistent with the location of the principal geometric discontinuities. The calculated vertical displacement generally increases from the lower restrained region toward the upper portion of the model. The maximum vertical displacement is

approximately 1.86 mm and occurs near the cantilevered spiral-case roof region at the 0° section. The maximum vertical displacements of the lower stay-ring corbel and the maintenance-gallery roof slab are approximately 0.55 mm and 0.98 mm, respectively. To assess whether these displacements are acceptable, they are compared with the serviceability limits adopted in the original code-based design. For the maintenance-gallery roof slab, the original design used an effective span of l_0 = 5.1 m and a permissible deflection of $[f] = l_0/400$ = 12.75 mm. The 3D FEA displacement is 0.98 mm, about 7.7% of this limit, and the simplified calculation gives 1.08 mm, also below the limit. For the lower stay-ring corbel, DL/T 5057-2009 does not prescribe a separate deflection limit for corbel-type discontinuity regions; its serviceability is governed mainly by crack width, local bearing, and ultimate capacity. For reference, applying the same conservative $l/400$ criterion to the corbel action distance of about 0.77 m gives 1.93 mm, and the computed 0.55 mm is below this value. Even under a stricter $l/500$ reference limit of 1.54 mm, the displacement remains acceptable. Thus, the computed displacements are within acceptable serviceability limits, and deformation does not govern the reinforcement design.

The horizontal displacement remains comparatively small throughout the analyzed region. The maximum value is approximately 0.73 mm, occurring near the upper spiral-case region at the 90° section, while the overall horizontal displacement remains below 0.8 mm. These results indicate that the global deformation response is limited under the prescribed design actions, although local deformation patterns reflect the three-dimensional interaction between the spiral case, stay-ring region, and surrounding concrete.

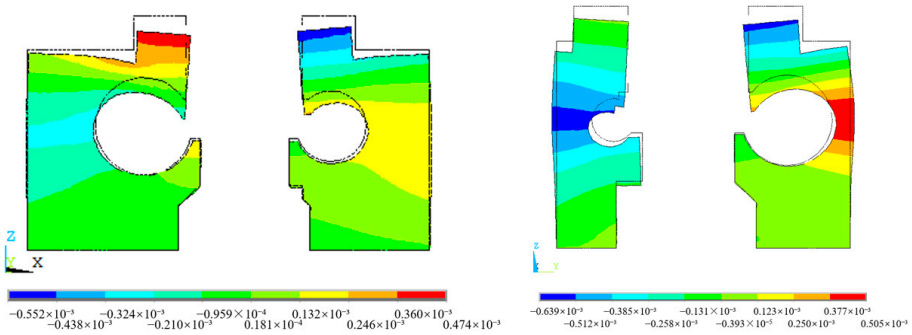
Representative vertical and horizontal displacement contours are summarized in Figure 9. In these displacement contour plots, warm colors (red/yellow) represent larger downward displacements or positive directional movements, whereas cool colors (green/blue) indicate smaller displacements or movement in the opposite direction. The unit of displacement in the legend is meters (m).



(a) Vertical-X (b) Vertical-Y

(c) Gallery-L (d) Gallery-T

Figure 9. *Cont.*



(e) Horizontal-X (f) Horizontal-Y

Figure 9. Representative displacement distributions obtained from the three-dimensional model.

4.3. Reinforcement Design Results

4.3.1. FEA-Based Reinforcement Design for the Stay-Ring Corbel

The finite element results identify the 0° section as the governing region for the tensile-stress-based reinforcement assessment of the lower stay-ring corbel. At this section, the effective tensile-zone depth occupies approximately $\frac{2.004-0.5}{2.004} = 0.75$ of the total section depth, exceeding two-thirds of the section depth. The tensile stresses within this region were integrated according to the procedure described in Section 3.3 to obtain the tensile resultant per unit circumferential width.

Based on the resulting tensile force and the adopted reinforcement design strength, the required reinforcement was determined and subsequently adjusted to satisfy detailing requirements. The adopted reinforcement arrangement is 5Φ28@200, corresponding to an effective reinforcement area of approximately 3079 mm^2/m. Circumferential reinforcement is retained principally for detailing and crack-control purposes.

The FEA-based reinforcement requirement is therefore substantially lower than that obtained from the conventional cantilever calculation, while the tensile reinforcement remains concentrated in the region indicated by the three-dimensional stress field. The quantitative difference is examined in Section 4.4.

4.3.2. FEA-Based Reinforcement Design Results for the Maintenance-Gallery Roof Slab

For the maintenance-gallery roof slab, the governing tensile region occurs at the bottom of the slab near midspan. The ratio of the effective tensile-zone depth to the total section depth is $\frac{1.2}{1.5} = 0.80$, which is also greater than two-thirds of the section depth. The tensile stress distribution was integrated over the effective region to obtain the tensile resultant per unit width.

The reinforcement demand calculated from the tensile resultant was subsequently adjusted to account for practical detailing requirements. The adopted bottom transverse reinforcement corresponds to approximately 3273 mm^2/m, while longitudinal reinforcement at the slab bottom is retained as detailing reinforcement.

As with the corbel, the FEA-based design indicates a more localized reinforcement demand than the conventional fixed-end beam calculation. The resulting difference in reinforcement area is quantified in Section 4.4.

4.4. Quantitative Comparison of Reinforcement Demand

The two design routes produce the same overall interpretation of the structural function of the stay-ring support system but lead to appreciable differences in the calculated reinforcement demand for the two critical regions.

For the lower stay-ring corbel, the simplified cantilever calculation results in a reinforcement area of approximately 4926 mm^2/m, whereas the tensile-stress-based finite element assessment gives approximately 3079 mm^2/m. The corresponding difference is approximately 37%.

For the maintenance-gallery roof slab, the simplified fixed-end beam calculation gives a midspan reinforcement area of approximately 4908 mm^2/m, compared with approximately 3273 mm^2/m from the finite element stress-field assessment. This corresponds to a difference of approximately 33%.

These results are summarized in Table 7. The percentage differences are specific to the investigated structural configuration and are presented here as quantitative outcomes of the two structural idealizations rather than as general reinforcement-reduction factors.

Table 7. Quantitative comparison of reinforcement demand.

Structural Region	Simplified Representation	Simplified Design	3D Representation	FEA-Based Design	Difference
Stay-ring corbel	Cantilever	4926 mm^2/m	3D continuum	3079 mm^2/m	−37%
Maintenance-gallery roof slab	Fixed-end beam	4908 mm^2/m	3D continuum	3273 mm^2/m	−33%

The observed differences originate from the different representations of structural behavior adopted by the two approaches. The simplified models convert spatial load transfer into equivalent member actions, whereas the continuum model allows stress redistribution through the surrounding concrete. The mechanical implications of these differences, together with the respective roles of the two design approaches, are discussed in Section 5.

5. Discussion

5.1. Influence of Structural Idealization on Load Transfer

The principal difference between the two design approaches lies not in the reinforcement formula itself, but in the way the structural system is represented before reinforcement demand is evaluated. The simplified calculation transforms the continuous three-dimensional concrete region into a sequence of mechanically interpretable members, including a Γ-shaped frame, a cantilever corbel, and a fixed-end beam. This representation enables sectional actions such as bending moment, shear force, and support reaction to be calculated explicitly and provides a transparent basis for code-based design. However, the conversion from a continuous three-dimensional region to individual members necessarily requires assumptions regarding effective span, load distribution, support conditions, and force-transfer paths.

The three-dimensional finite element model retains the geometric continuity of the stay-ring support region and therefore permits load transfer through multiple interacting paths. This distinction is particularly important in the lower stay-ring corbel. In the simplified calculation, the reaction transferred from the stay ring is converted into an equivalent line load acting on a cantilever member. The resulting bending and shear actions are then used to design reinforcement over the governing section. In the continuum model, by contrast, part of the applied action is redistributed through the surrounding concrete and adjacent restrained regions. Consequently, the tensile demand is concentrated within a more localized zone rather than being represented by a sectional action distributed over the entire idealized member.

A similar mechanism is observed in the maintenance-gallery roof slab. The simplified calculation treats the roof as a fixed-end beam spanning between two thick walls. This ide-

alization produces relatively large sectional bending moments at the midspan and supports. In the three-dimensional model, however, the slab remains mechanically connected to the adjacent mass concrete and surrounding walls, allowing part of the load to be transferred through spatial restraint and local stress redistribution. The resulting tensile demand at the midspan is therefore more localized than that implied by the equivalent beam model.

These findings support the broader observation that complex reinforced-concrete regions cannot always be represented uniquely by conventional member actions. Previous studies of disturbed regions have similarly shown that local force transfer and reinforcement demand are strongly influenced by the adopted structural idealization and stress-field representation [16–18]. These observations are consistent with recent studies showing that contact/gap-closing behavior and temporary internal water pressure significantly affect load sharing between steel and concrete in spiral case structures [6,7,9].

5.2. Interpretation of the Differences in Reinforcement Demand

The quantitative comparison shows that the reinforcement demand obtained from the three-dimensional stress-field assessment is approximately 37% lower for the stay-ring corbel and 33% lower for the maintenance-gallery roof slab than that obtained from the corresponding member-based calculations. These differences are substantial, but they should not be interpreted as evidence that three-dimensional finite element analysis universally leads to a similar reduction in reinforcement.

Instead, the observed differences arise from the cumulative influence of several modeling choices. First, the simplified approach reduces a continuous three-dimensional structural region to one- or two-dimensional members. Second, spatially distributed actions are converted into equivalent sectional or line loads. Third, restraint provided by the surrounding mass concrete is represented by idealized support conditions. Fourth, localized tensile stress fields are transformed into global sectional actions such as bending moments and shear forces. Each of these simplifications is reasonable from the perspective of conventional engineering design, but their combined influence can increase the resulting reinforcement demand in geometrically disturbed regions.

For the stay-ring corbel, the cantilever idealization concentrates the transferred reaction at the corbel level and treats the section as carrying the resulting bending and shear in a conventional member sense. The three-dimensional model instead indicates that the tensile stress is concentrated mainly near the upper region adjacent to the spiral-case cavity. This difference in load-path representation explains why the required reinforcement derived from the continuum stress field is smaller than that obtained from the cantilever calculation.

For the maintenance-gallery roof slab, the beam idealization similarly assigns the entire span response to a one-dimensional bending mechanism. In the three-dimensional model, part of the applied action is redistributed toward the side walls and surrounding concrete. The reduced midspan tensile demand therefore reflects the spatial support conditions rather than a simple reduction in design conservatism.

Accordingly, the values of 37% and 33% should be regarded as case-specific outcomes of the investigated geometry, load combinations, boundary conditions, and design provisions, rather than as transferable reduction coefficients for other hydropower structures. The significance of the comparison lies in demonstrating that the level of structural idealization can materially influence reinforcement decisions in complex three-dimensional concrete regions. These differences are conditional on the linear-elastic idealization and should not be treated as post-cracking reinforcement-reduction factors. Comparable differences between simplified code-based design and refined FEA have also been reported for skewed slab bridges [13]; however, the present structure is a three-dimensional D-region with large openings and embedded components, so the reported percentages remain case-specific.

5.3. Complementary Roles of Simplified Calculation and Three-Dimensional FEA

These findings should not be interpreted as advocating the replacement of simplified structural calculations by finite element analysis. The member-based approach retains several important advantages in practical engineering design. Its assumptions are explicit, the load path can be independently reproduced, and the governing sectional actions can be directly checked against design-code requirements. These characteristics make simplified calculations particularly useful for preliminary sizing, scheme comparison, independent checking, and overall design control. This role is consistent with the motivation stated earlier in the manuscript, where transparency, computational efficiency, and ease of verification were identified as principal strengths of member-based design.

Three-dimensional FEA serves a different function. Its main advantage in the present study is that it preserves the continuity of the structural geometry and provides direct information on local stress transfer, spatial restraint, and stress concentration. This is particularly useful for disturbed regions containing large openings, abrupt changes in section, embedded steel components, or irregular support conditions. Related studies on complex concrete systems have likewise shown that refined finite element models can provide structural information that is difficult to capture using conventional member idealizations alone [11,12].

The two approaches should therefore be regarded as complementary rather than competing design tools. A practical design workflow is to use simplified calculations to establish the principal load path, identify governing sections, and provide a transparent code-based baseline. Refined three-dimensional analysis can then be used for geometrically disturbed regions where the adequacy of the member idealization is uncertain or where local reinforcement detailing depends strongly on the spatial stress field.

This interpretation also clarifies the role of the tensile-stress-region approach adopted in this study. Rather than using FEA merely to generate stress contours, the calculated tensile field is connected directly to reinforcement assessment. Similar stress-field-based reinforcement concepts have been applied to anchorage zones, gussets, and other D-regions in reinforced concrete structures [16–18]. Thus, the engineering value of the finite element model lies not in replacing conventional design calculations, but in providing additional information where member-based sectional forces are difficult to define.

5.4. Engineering Implications and Limitations

From an engineering perspective, the present results suggest that refined three-dimensional analysis can help identify where reinforcement demand is concentrated and where conventional member-based assumptions may introduce additional conservatism. For complex hydropower concrete structures, this may support more targeted reinforcement detailing and reduce unnecessary concentration of reinforcement in regions where the actual tensile demand is spatially limited. However, the present study does not include a full cost analysis; therefore, the observed reductions in reinforcement area should be interpreted as potential material savings rather than demonstrated economic benefits.

Several limitations should also be recognized. First, the finite element model was not calibrated against physical model tests, full-scale experiments, or field-monitoring data. The numerical results should therefore be interpreted as a refined design-level representation under the prescribed modeling assumptions rather than as direct experimental validation of the actual structural response.

Second, the analysis adopted a linear-elastic material representation, which is consistent with the stress-based procedure in DL/T 5057-2009 but does not explicitly simulate cracking, stiffness degradation, tension stiffening, bond-slip, or force redistribution. Cracking-induced redistribution and contact separation were not modeled. Previous studies

have shown that cracking, gap closure and interface separation can significantly change stress and load-sharing in hydraulic concrete structures [6,7,9]. Cracking can reduce local elastic tensile peaks, but it does not necessarily reduce reinforcement demand. Once concrete cracks, tensile force is transferred to reinforcement and adjacent uncracked regions; for serviceability, crack width, crack spacing, and long-term effects may govern. Cracking-induced stiffness degradation can also change global load distribution, either relieving or increasing demand in the regions considered. For the maintenance-gallery roof slab, the simplified calculation already gives a maximum crack width of 0.29 mm, close to the 0.30 mm limit; if cracking-induced redistribution increases local reinforcement stress, crack-width control could govern, and the FEA-based reduction might not be fully attainable. The FEA values of 3079 and 3273 mm^2/m are therefore elastic stress-based estimates, and the 37% and 33% differences should not be interpreted as post-cracking reduction factors. Nonlinear cracking analysis, tension stiffening, bond-slip, or sensitivity studies would be desirable. In practical design, the elastic tensile-stress regions remain useful for locating crack-control reinforcement, but any reduction relative to the simplified calculation should be accepted only after serviceability checks and detailing requirements are satisfied.

Third, the design provisions and partial factors adopted in this study are those of DL/T 5057-2009, which has been superseded by NB/T 11011-2022. The comparison results are therefore conditioned on the older code provisions. Although the principal material strength parameters and the stress-based reinforcement assessment framework are unchanged between the two code versions, the increase in partial factors in NB/T 11011-2022 would increase the absolute reinforcement demand in both calculation routes. The relative differences reported in this study, however, are governed by the structural idealization and load-transfer representation rather than by the partial factor values, and are therefore expected to remain broadly valid under the revised code.

Fourth, the study is based on a single structural configuration. The observed reinforcement differences depend on the specific geometry, support conditions, load-transfer path, and design provisions of the investigated stay-ring support system. The reported differences of approximately 37% and 33% should therefore not be generalized to other hydropower powerhouse structures without additional analysis.

Finally, the numerical model retained the original engineering discretization and boundary assumptions. No independent mesh-convergence, boundary-sensitivity, or parametric analysis was performed within the scope of the present comparative study. Since the reinforcement demand was evaluated from the integrated tensile resultant, the results are less sensitive to local mesh refinement than peak-stress-based assessments. However, mesh discretization may still influence the predicted extent of the tensile zone. These aspects may be examined in future work together with nonlinear analysis, field measurements, or physical-model testing.

6. Conclusions

This study compared a conventional member-based structural calculation with a three-dimensional finite element approach for the reinforcement design of a geometrically complex stay-ring support structure in a hydropower powerhouse. The main conclusions are as follows.

(1) The two approaches represent the same structural system at different levels of abstraction. The simplified calculation transforms the continuous concrete region into mechanically interpretable members, including a Γ-shaped frame, a cantilever corbel, and a fixed-end beam, thereby providing a transparent basis for code-based sectional design. In contrast, the three-dimensional finite element model retains the geometric continuity of the

surrounding concrete and provides additional information on spatial restraint, local stress concentration, and load redistribution.

(2) The three-dimensional analysis identifies localized tensile demand in the connection region between the spiral-case roof and the stay-ring support. The calculated tensile stress reaches approximately 7.54 MPa in the most pronounced local region, while the lower stay-ring corbel and the maintenance-gallery roof slab exhibit maximum tensile stresses of approximately 2.42 MPa. The calculated deformation remains limited under the prescribed design actions, with maximum vertical displacements of approximately 0.55 mm for the corbel and 0.98 mm for the gallery roof slab, which are within the adopted serviceability limits and do not govern the reinforcement design.

(3) The different structural representations lead to appreciable differences in reinforcement demand. For the lower stay-ring corbel, the simplified cantilever calculation gives a reinforcement area of approximately 4926 mm^2/m, compared with approximately 3079 mm^2/m from the tensile-stress-based finite element assessment, corresponding to a difference of about 37%. For the maintenance-gallery roof slab, the corresponding values are approximately 4908 and 3273 mm^2/m, giving a difference of about 33%. These differences are attributed primarily to the treatment of spatial load redistribution, support restraint, and localized tensile demand and should be regarded as case-specific rather than as general reinforcement-reduction factors.

(4) Simplified structural calculations and three-dimensional finite element analysis should be regarded as complementary rather than competing design tools. The former is well suited to establishing principal load paths, governing sectional actions, and transparent code-based design checks, whereas the latter is particularly useful for disturbed regions in which three-dimensional interaction and local stress transfer cannot be readily represented by conventional member models.

(5) The present study is limited by the use of a single engineering case, a linear-elastic finite element representation, and the absence of independent experimental or field-based model calibration. The numerical results therefore represent a design-level comparative assessment rather than direct validation of the complete structural response. Future studies may incorporate nonlinear cracking analysis, field measurements, physical testing, or sensitivity analyses to further examine the robustness and generality of the observed load-transfer mechanisms. The numerical results therefore represent a design-level comparative assessment rather than direct validation of the complete structural response. In addition, the design provisions adopted in this study correspond to DL/T 5057-2009; although this code has been superseded, the core material parameters and the stress-based reinforcement assessment framework are unchanged in the current NB/T 11011-2022, so the comparative conclusions are not expected to be materially affected by the code revision. Nevertheless, cracking was not explicitly modeled, so the computed tensile stresses and reinforcement demands are elastic estimates. Cracking-induced redistribution may alter tensile demand and make crack-width control govern; therefore, the reported differences of about 37% and 33% should not be treated as general post-cracking reduction factors. Future work should include nonlinear cracking and sensitivity analyses.

Author Contributions: Conceptualization, H.W. and T.N.; Methodology, H.W. and T.N.; Formal Analysis, Y.Z.; Investigation, Y.Z. and H.W.; Resources, T.N.; Data Curation, Y.Z.; Writing—Original Draft Preparation, Y.Z.; Writing—Review and Editing, H.W. and T.N.; Visualization, Y.Z.; Supervision, H.W. and T.N.; Project Administration, H.W. and T.N. All authors have read and agreed to the published version of the manuscript.

Funding: This research was funded by 2024–2026 Sichuan Province Higher Education Talent Cultivation Quality and Teaching Reform Project (grant number JG2024-0600), and by 2024–2026 Chengdu University of Technology Higher Education Talent Cultivation Quality and Teaching Reform Project (grant numbers 73 and 10800-000098322).

Data Availability Statement: The datasets presented in this article are not readily available because they contain confidential engineering information on the hydropower project. Requests to access the datasets should be directed to the corresponding author.

Acknowledgments: The authors would like to thank the engineering institute for providing relevant project documentation and technical support for this study.

Conflicts of Interest: Author Hao Wen was employed by the company PowerChina Guiyang Engineering Corporation Limited. The remaining authors declare that the research was conducted in the absence of any commercial or financial relationships that could be construed as a potential conflict of interest.

References

1. Abdelwahed, B.S. Analytical and Modeling Studies on Discontinuity Regions in Reinforced Concrete Elements: Review Article. *Innov. Infrastruct. Solut.* **2026**, *11*, 207. [CrossRef]
2. Abbood, A. Strut-and-Tie Model and Its Applications in Reinforced Concrete Deep Beams: A Comprehensive Review. *Case Stud. Constr. Mater.* **2023**, *19*, e02643. [CrossRef]
3. Wei, K.L.; Zhang, F.J.; Zhang, Y.; Yang, Y.; Wang, X.Y. A Method for Seismic Resistance of Reinforced Concrete Structures in Agricultural Water Conservancy Projects. *Pak. J. Agric. Sci.* **2023**, *60*, 537–548. [CrossRef]
4. Wan, D.; Xiao, Q. Finite Element Analysis of Structural Stability of Surge Chamber in Changbo Hydropower Project. *Sichuan Water Power* **2025**, *44*, 130–134. (In Chinese) [CrossRef]
5. Zhang, Q.L.; Hu, L.; Gao, X.F. Fatigue Life Prediction of Steel Spiral Cases in Pumped-Storage Power Plants: Factors to Be Considered. *Eng. Fail. Anal.* **2024**, *157*, 107908. [CrossRef]
6. Gao, X.F.; Wu, H.G.; Fu, D. Effect of Temporary Internal Water Pressure on Structural Performance of Spiral Case Structure in Pumped-Storage Power Plants. *Energies* **2022**, *15*, 2463. [CrossRef]
7. Hu, L.; Xiang, A.-J.; Liu, D.; Fu, D.; Li, H.; Hu, X. Inconsistent Gap-Closing Behavior of Spiral Case Structures in Hydropower Stations: Mechanism and Structural Role. *KSCE J. Civ. Eng.* **2025**, *29*, 100156. [CrossRef]
8. Zhao, Y.; Li, X.J.; Lu, Y.G.; Dong, H.Y.; Sun, C.Z.; Wang, Z.W. Stability Study and Strengthening Strategy of Spiral Case-Encased Concrete Structure of Pumped Storage Power Station. *Water* **2024**, *16*, 2687. [CrossRef]
9. Zhou, Y.F.; Su, K.; Wu, H.G. Hydro-Mechanical Interaction Analysis of High Pressure Hydraulic Tunnel. *Tunn. Undergr. Space Technol.* **2015**, *47*, 28–34. [CrossRef]
10. Wang, T.; Liu, Z.; Meng, J.; Li, M.; Wang, W. Steel Reinforced CA-UHPC One-Way Slabs: Experimental Study, Numerical Simulation, and Bridge Deck Application. *Constr. Build. Mater.* **2026**, *518*, 145746. [CrossRef]
11. Jia, S.Z.; Cao, W.L.; Zhang, Y.C.; Yuan, Q. Simplified Calculation Model and Finite-Element Analysis of Frame-Supported Ribbed-Grid Composite Slab Structure. *KSCE J. Civ. Eng.* **2018**, *22*, 3383–3394. [CrossRef]
12. Tan, J.K.; Zheng, W.L.; Wang, Y.H.; Su, M.N.; Zhao, L.; Zhang, Y.H.; Feng, Y.; Chen, D.X. Finite Element Modelling and Design of Concrete Wind Turbine Towers Subjected to Combined Compression and Bending. *Structures* **2025**, *77*, 108811. [CrossRef]
13. Moya, L.; Lantsoght, E.O.L. Parametric Study on the Applicability of AASHTO LRFD for Simply Supported Reinforced Concrete Skewed Slab Bridges. *Infrastructures* **2021**, *6*, 88. [CrossRef]
14. Thoma, K.; Roos, P.; Borkowski, G. Finite Element Analysis of Reinforced Concrete Slabs—Post-Test Calculations of Plate Tests Using the Cracked Membrane Model. *BETON- UND STAHLBETONBAU* **2014**, *109*, 895–904. [CrossRef]
15. Gall, V.E.; Marwan, A.; Smarslik, M.; Obel, M.; Mark, P.; Meschke, G. A Holistic Approach for the Investigation of Lining Response to Mechanized Tunneling Induced Construction Loadings. *Undergr. Space* **2018**, *3*, 45–60. [CrossRef]
16. Liu, C.; Xu, D.; Jung, B.; Morgenthal, G. Reinforcement Design for the Anchorage of Externally Prestressed Bridges with Tensile Stress Region. *Comput. Concr.* **2013**, *11*, 383–397. [CrossRef]
17. Nie, Y.H.; Zhang, J.; Liu, D.L.; Lan, T.Y.; Xiao, D.; Xiong, M.; Dong, Z.F. Strut-and-Tie Model and Reinforcement Design Method for Gusset in the Containment Vessel. *Structures* **2024**, *65*, 106693. [CrossRef]
18. He, L.Y.; Xiong, X.Y.; Bao, L.J. Full-Scale Test and Strut-and-Tie Model of Thick Plate Multiple Block Anchorage Zone. *Eng. Struct.* **2025**, *334*, 120251. [CrossRef]
19. *DL/T 5057-2009*; Code for Design of Hydraulic Concrete Structures. China Electric Power Press: Beijing, China, 2009.

20. *DL/T 5077-1997*; Code for Load Design of Hydraulic Structures. China Electric Power Press: Beijing, China, 1997.
21. *Standard's NB/T 11011-2022*; Code for Design of Hydraulic Concrete Structures. China Water & Power Press: Beijing, China, 2022.

Disclaimer/Publisher's Note: The statements, opinions and data contained in all publications are solely those of the individual author(s) and contributor(s) and not of MDPI and/or the editor(s). MDPI and/or the editor(s) disclaim responsibility for any injury to people or property resulting from any ideas, methods, instructions or products referred to in the content.